NANO LETTERS

LETTER

pubs.acs.org/NanoLett

Optical and Topological Characterization of Gold Nanoparticle Dimers Linked by a Single DNA Double Strand

Mickaël P. Busson,[†] Brice Rolly,[‡] Brian Stout,[‡] Nicolas Bonod,[‡] Eric Larquet,[§] Albert Polman,[∥] and Sébastien Bidault*[,†]

[†]Institut Langevin, ESPCI ParisTech, CNRS UMR 7587, INSERM U979, 10 rue Vauquelin, 75005 Paris, France

[‡]Institut Fresnel, CNRS UMR 6133, Ecole Centrale Marseille, Aix-Marseille Université, Domaine Universitaire de Saint Jérôme, 13397 Marseille, France

[§]Département de Biologie Structurale, Institut de Minéralogie et de Physique des Milieux Condensés, CNRS UMR 7590, Université Pierre et Marie Curie Paris VI, 75005 Paris, France

[∥]Center for Nanophotonics, FOM Institute AMOLF, Science Park 104, 1098 XG Amsterdam, The Netherlands

Supporting Information

ABSTRACT: We demonstrate that symmetric or asymmetric gold nanoparticle dimers with substantial scattering cross sections and plasmon coupling can be produced with a perfectly controlled chemical environment and a high purity using a single DNA linker as short as 7 nm. A statistical analysis of the optical properties and morphology of single dimers is performed using darkfield and cryo-electron microscopies. These results, correlated to Mie theory calculations, indicate that the particle dimers are stretched in water by electrostatic interactions.

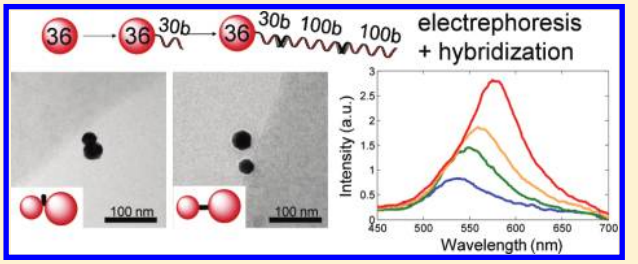

KEYWORDS: Nanoparticle dimers, plasmon coupling, DNA self-assembly, cryo-electron microscopy, darkfield microscopy, Mie theory

Gold nanoparticles (AuNPs) have been extensively studied as photothermal[1,2] and optical contrast agents[3,4] thanks to their large absorption and scattering cross sections at visible plasmon resonance frequencies. Functionalizing AuNPs with DNA strands is a powerful tool to drive the assembly of groupings with optical properties that strongly depend on the distance between particles.[5,6] This approach was successfully applied to the design of biosensors,[7−9] molecular rulers,[10−14] and enhancers of Raman scattering[15−17] or fluorescence emission.[18] For all these applications, it is desirable to fully control the chemical environment of the nanostructure and, in particular, to define the number of DNA strands grafted to each particle. Agarose gel electrophoresis,[19] and more recently high-performance liquid chromatography (HPLC),[20] were shown to allow the purification of gold nanoparticles linked to a known number of thiolated DNA single strands. Hybridization then drives the assembly of well-defined particle groupings.[21−28] However, the stability of gold colloidal suspensions has limited this approach to particles smaller than 20 nm in diameter.[20] Furthermore, for 20 nm diameter particles, electrophoretic purification only works when the grafted DNA strand is of the order of 90 or 100 bases.[20,27] Applications of AuNP groupings in sensing, in imaging, and in surface enhanced spectroscopy require nanostructures with non-negligible scattering cross sections and plasmon coupling. The particle diameters should thus be larger than 30 nm[10−14] and the interparticle gaps, and therefore the DNA spacers, should be shorter than the particle radii;[29−31] conditions that have not been achieved so far in the literature with a controlled number of DNA strands.

In this report, we study the efficient purification of AuNPs as large as 36 nm in diameter grafted to a known number of DNA strands as short as 10 nm using gel electrophoresis. We then combine particles of different or identical sizes linked to cDNA strands to produce high purity dimer suspensions that are characterized in cryo-electron microscopy (cryo-EM). Since the obtained groupings exhibit significant scattering cross sections, they can also be characterized individually by darkfield confocal spectroscopy for different DNA linkers to correlate interparticle gaps and plasmon resonance wavelengths.

The conjugation of a limited number of thiolated DNA strands on the surface of gold nanoparticles is performed following several ligand exchange steps, as described in the literature.[12,19] In order to minimize nonspecific interactions between the negatively charged DNA strands and the metal surface and to optimize colloidal stability, AuNPs are prepared with a negatively charged phosphine shell (all experimental conditions and DNA sequences are given in the Supporting Information). This labile ligand can be displaced by thiolated DNA strands in the presence of charge screening cations (typically Na^+). However, colloidal stability of phosphine stabilized AuNPs larger than 30 nm in

Received: September 14, 2011
Revised: October 18, 2011
Published: October 19, 2011

diameter is only optimum for NaCl concentrations lower than 50 mM. The ionic strength during AuNP conjugation is chosen at 30 mM NaCl as a compromise between colloidal stability and sufficient charge screening to graft the thiolated DNA strands on the gold surface. In order to further stabilize the AuNP−DNA conjugates, the gold surface is passivated by adding a large excess of short thiolated poly(ethylene glycol) (PEG) oligomers before the electrophoretic purification. To minimize removal of the thiolated DNA strands by the large excess of PEG molecules, the chemical linker added at the 3′ or 5′ end of the DNA strand exhibits three thiol moieties as discussed in several publications.[12,20,32]

Electrophoretic purification of AuNP−DNA conjugates relies on sufficient differences in conjugate size and/or surface charge to drive the appearance of well-separated bands. In the case of gold particles with 5 nm diameters, this occurs with DNA strands as short as 50 bases,[19] but for AuNPs larger than 30 nm in diameter, the grafted DNA strands need to be longer than several hundred bases. Figure 1a shows the end result of the electrophoretic purification of 36 nm gold particles after interaction with trithiolated 30 bases long DNA single strands (see Supporting Information for the experimental conditions). Lane 1 corresponds to a reference sample of 36 nm AuNPs after passivation with thiolated methyl terminated PEG molecules indicating a net negative charge (the arrow indicates the diffusion direction of the conjugates toward the anode). The second lane shows the product of identical particles after overnight reaction with a 33-fold excess of DNA strands in a 30 mM NaCl solution. A single, slightly slower band is observed. Even though the slower diffusion speed can indicate an increased conjugate volume resulting from DNA functionalization, it is difficult to estimate the number of grafted strands. In order to effectively increase the length of the linked oligo, we follow the scheme described in Figure 1a: the trithiolated DNA sequence is hybridized over 15 bases with a 100 bases strand which can be further lengthened by adding subsequent 100 bases long molecules also hybridized over 15 bases. All DNA sequences are designed to ensure that hybridization of the different strands occurs in a controlled order (see Supporting Information for the sequences). In particular, the 70 unhybridized bases of the lengthening DNA molecules are thymine to minimize nonspecific interactions between the different single strands. This scheme was demonstrated once in the literature with one lengthening DNA strand but only with AuNPs smaller than 10 nm in diameter.[28] The lengthening DNA strands are added in excess to ensure that all thiolated DNA molecules are hybridized to the same number of oligos. Furthermore, the thiolated and lengthening strands are mixed in a 40 mM NaCl solution and then heated to 85 °C and left to cool overnight before adding the gold particles (see Supporting Information). Lanes 3−7 in Figure 1a show the electrophoretic purification of 36 nm gold particles after overnight incubation with the target thiolated DNA molecule hybridized to an increasing number of 100 bases long single strands (from one to five). While separate bands start appearing for three lengthening strands (lane 5), weakly overlapping bands are only obtained for five extra DNA molecules (lane 7).

These experiments were performed with either 30 or 50 bases long and 3′ or 5′ thiolated target sequences. Furthermore, 27 nm diameter particles can also be efficiently attached to short DNA strands by adding four 100 bases long lengthening molecules. It is interesting to note that the large excess of lengthening DNA strands also increases the stability of AuNPs in salt containing solutions. This nonspecific interaction of DNA single strands with metallic particles was discussed in previous reports.[33,34] In practice, to avoid aggregation in the samples where less than three lengthening strands are added (lanes 2−4 of Figure 1a), we added a large excess of an unmodified 100 bases long DNA molecule that does not hybridize to the target thiolated strand or any other involved oligonucleotide.

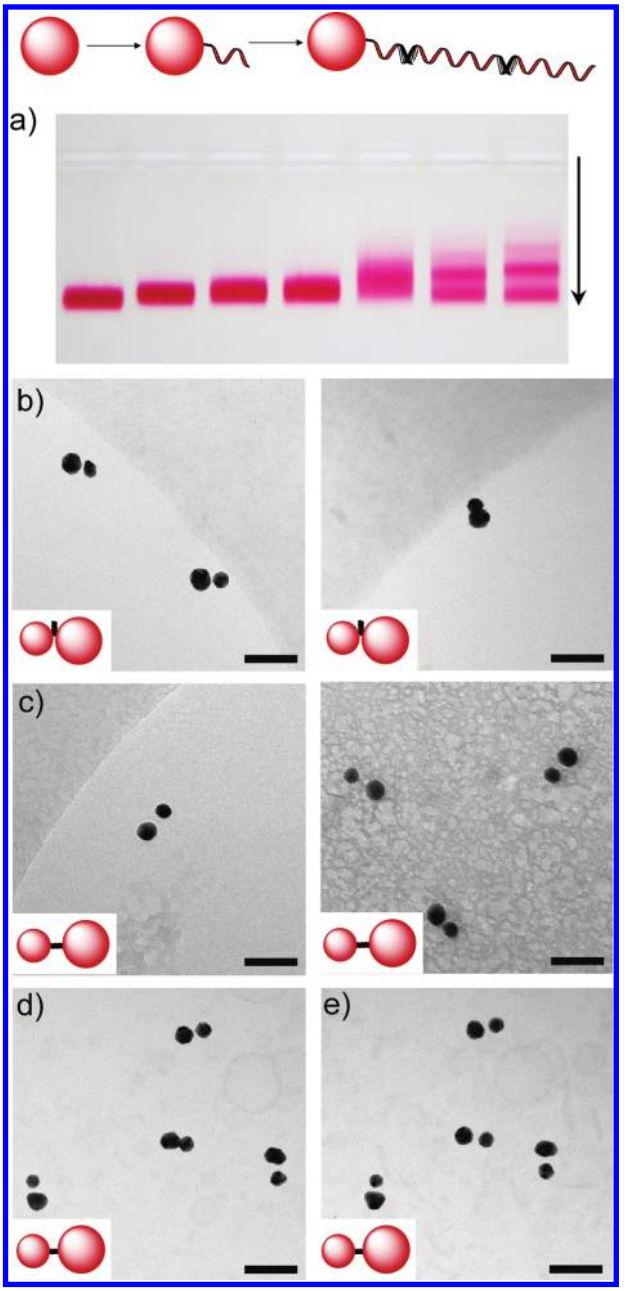

Figure 1. (a) Scheme for the effective lengthening of a thiolated DNA strand grafted on a AuNP. The photograph shows the electrophoretic purification of 36 nm diameter AuNPs after interaction with a 30 bases long DNA strand hybridized to 0−5 lengthening 100 bases long strands (lanes 2−7) compared to a reference nanoparticle sample (lane 1). (b−e) Cryo-EM images of asymmetric 27−36 nm AuNP dimers (scale bar = 100 nm). (b) 50 bp DNA linker perpendicular to the dimer axis. (c) 50 bp DNA linker parallel to the dimer axis. (d, e) 30 bp DNA linker parallel to the dimer axis with the electron beam perpendicular (d) or with a 45° angle with regard to the sample plane (e). Insets: sketches of the different sample geometries.

dx.doi.org/10.1021/nl2032052 |*Nano Lett.* 2011, 11, 5060–5065

The relative density of the different bands in lane 7 strongly depends on the excess concentration of DNA strands versus AuNPs (see Supporting Information), demonstrating that they are a result of DNA functionalization with each band corresponding to an extra attached molecule. Separation of conjugates preferentially linked with up to four DNA strands per particle is possible before the bands corresponding to extra grafted molecules start to overlap. In this report, we optimized the preparation conditions for monoconjugated AuNPs as in Figure 1a (second band from the bottom in lanes 6 and 7). Following published procedures,[19,27] the band is cut from the gel and the conjugate is eluted into running buffer before being concentrated by centrifugation for the subsequent hybridization. To remove the lengthening strands and facilitate hybridization, the monoconjugates with cDNA sequences are mixed in 40 mM NaCl, heated to 55 °C, and allowed to cool overnight. The melting temperature of a 15 base pairs (bp) DNA strand is around 40−45 °C and should be similar to the melting temperature of two consecutive lengthening strands also hybridized over 15 bases. A second electrophoretic purification separates unreacted conjugates from hybridized dimers for symmetric or asymmetric geometries (see Supporting Information). A faint trimer band is also observed in the agarose gel indicating that our purification process does not remove 100% of multiconjugated AuNPs. This is always obtained for electrophoresis based separation techniques compared to HPLC which allows higher purities but requires high NaCl concentrations[20] difficult to combine with the colloidal stability of large AuNPs.

Purified suspensions of AuNP dimers are characterized in electron microscopy. Since groupings of AuNPs larger than 10 nm in diameter tend to aggregate when dried on TEM grids,[20] we perform experiments in cryogenic conditions. This technique allows the characterization of nanoparticle groupings as they are in solution without the influence of drying effects or substrate interactions.[35,36] The colloidal suspension is blotted on holey carbon-coated copper grids before being frozen rapidly in liquid ethane to obtain a thin vitreous water film that weakly scatters the electron beam compared to AuNPs. To ensure that the imaged groupings are not obtained from nonspecific aggregation, the characterized dimers are asymmetric: composed of 27 and 36 nm diameter AuNPs. Panels b−e of Figures 1 show cryo-EM images of synthesized dimers for different DNA linkers. Figure 1b corresponds to a 50 bp linker that is perpendicular to the dimer axis: one particle is linked on the 5′ end of one strand while the other is grafted on the 3′ end of the complementary strand (see the inset sketch). Dimers obtained with the same DNA sequence but with particles attached at the 5′ ends of both strands are shown in Figure 1c. Finally, Figure 1d corresponds to dimers with a 30 bp DNA linker with thiol moieties at the 5′ ends. Since the vitreous water film formed on the carbon grid is several tens of nanometers thick,[35,36] the imaged interparticle gap strongly depends on the angle between the electron beam and the sample. This is demonstrated in Figure 1e which corresponds to the same dimers as in Figure 1d with the sample plane tilted by 45°. The two-dimensional projection of a three-dimensional sample makes estimating the distributions of interparticle gaps difficult as it will be discussed in the following paragraphs in correlation to the optical measurements. The dimer purities of the samples shown in panels b, c, and d of Figure 1 are 48%, 68% and 73%, respectively (see Supporting Information for extra cryo-EM images, including low magnification ensemble images). The rest of the sample consists of single 36 nm particles (the 27 nm particles are better separated from the dimers in electrophoresis) and less than 7% of larger aggregates.

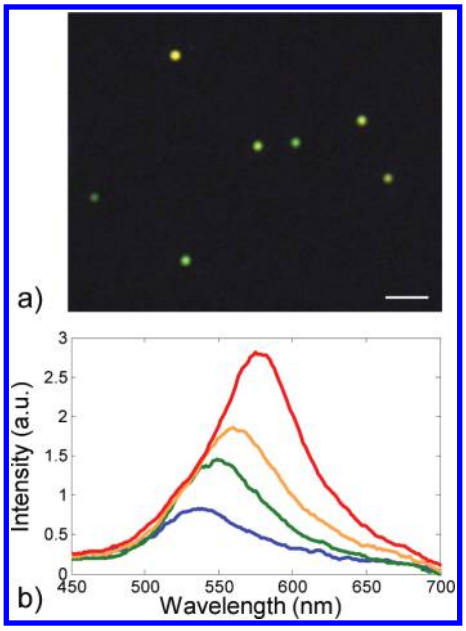

Figure 2. (a) Color CCD darkfield image of 36 nm AuNP dimers with a 50 bp DNA linker perpendicular to the dimer axis in microfluidic conditions (scale bar = 5 μm, 0.5 s integration time). (b) Representative scattering spectra of single 36 nm AuNPs (blue line) and AuNP dimers with different DNA scaffolds: 50 bp DNA linker parallel to the dimer axis (green line), 30 bp DNA linker parallel to the dimer axis (orange line), 50 bp DNA linker perpendicular to the dimer axis (red line). The arbitrary units correspond to the same integration time and EMCCD gain on the detector after background subtraction and spectral correction of the white light illumination.

Since AuNP dimers exhibit extinction spectra that depend strongly on small changes in particle size, shape, or interparticle gaps, ensemble measurements will not provide accurate information on small modifications of the DNA linker. However, scattering spectra of single gold particles larger than 30 nm in diameter can be readily estimated in darkfield microscopy as discussed in previous publications.[10−14] As aforementioned, gold particle dimers are sensitive to high ionic strengths, drying effects, and interactions with a substrate. To minimize these effects, the particle groupings are kept in suspension during the optical measurements. We thus use published protocols to functionalize the walls of homemade microfluidic chambers with NeutrAvidin.[12] The thiolated PEG shell of one of the two particles composing the dimer is then modified to exhibit biotin molecules that attach specifically to NeutrAvidin (see Supporting Information).[12] As discussed in several reports,[10−14] this allows the specific attachment of one particle of the AuNP dimers on the glass substrate while keeping the other in suspension. A darkfield image of a symmetric 36 nm AuNP dimer sample is shown in Figure 2a for the DNA linker geometry of Figure 1b. We use symmetric dimers to optimize the scattering cross sections compared to the asymmetric groupings shown in Figure 1 (the scattering cross section of a 36 nm AuNP is 5.6 times larger than that of a 27 nm particle). Figure 2a shows that the low grouping concentration used in our experiments allows us to avoid finding several dimers in the same focal volume. Representative scattering spectra from 36 nm diameter AuNP dimers for the different DNA linker lengths and geometries are given in Figure 2b compared to a single

dx.doi.org/10.1021/nl2032052 |Nano Lett. 2011, 11, 5060–5065

particle. The optical data treatment is identical for the different spectra and accounts for both local background signal modifications and the spectrum of the halogen lamp. Figure 2b shows that AuNP dimers exhibit larger scattering cross sections and red-shifted resonance wavelengths compared to single particles and that both effects increase as the DNA linker shortens. This is the expected optical response of metallic particle pairs that is dominated by the dipolar longitudinally coupled plasmon mode. It was already observed in gold[9−14] and silver[37,38] particle dimers in which the number of grafted biomolecules was not controlled. The orientation of particle dimers in the sample plane can also be estimated in darkfield microscopy using polarization-dependent measurements.[9,14,37,38] However, studying the resonance wavelengths is sufficient when investigating only the interparticle distances .[29−31]

Several tens of spectra from scattering objects for the different dimer samples were measured (185 spectra in total). We filter out 6% of the spectra which exhibit resonance wavelengths larger than 620 nm or several resonance peaks, indicating large aggregated groupings and/or strongly nonspherical particles.[11] For the dimer samples, we neglect scatterers with cross sections corresponding to a single particle sample, accounting for between 26 and 29% of the data for the different dimer geometries. This relative amount of single particles is similar to the one observed in cryo-EM images. The resonance wavelength distribution from the remaining 67% of the measurements is given in Figure 3 alongside the distributions of interparticle distances estimated from the cryo-EM images. Panels a(i) and b(i) of Figure 3 correspond to a 50 bp DNA linker perpendicular to the dimer axis (see Figure 1b). Panels a(ii) and b(ii) and a(iii) and b(iii) in Figure 3 are obtained using a 30 and a 50 bp DNA linker, respectively, with thiolated 5′ ends (Figure 1, panels d/e and c for the 30 bp and 50 bp strands, respectively). The diameter distributions of the 27 and 36 nm AuNPs are given in Figure 3a(iv). Finally, the resonance wavelength distribution measured in a sample prepared with single 36 nm particles is shown in Figure 3b(iv). Two main conclusions can be drawn from this figure: a shortened DNA linker is correlated to red-shifted dimer resonance wavelengths but the sample exhibits wide distributions in both geometry and optical responses.

The measured distributions of interparticle distances are obtained by analyzing automatically the cryo-EM images and estimating the center to center distance between two circles that best fit the AuNPs. The widths of the distributions arise from three contributions: distributions of particle diameters, distribution of interparticle gaps, and projection of the dimer axis on the plane perpendicular to the electron beam. This last factor cannot be neglected as shown on Figure 1: a partial superposition of the two particles is observed on several cryo-EM images and would correspond to negative gaps if measured directly. A full three-dimensional tomographic reconstruction of each dimer would correct for this projection and narrow the observed distance distributions. The distributions of the particle diameters are given in Figure 3a(iv) by fitting the AuNPs in all cryo-EM images with circles. The solid curves given in panels a(i−iii) of Figure 3 correspond to Gaussian distributions of the unknown interparticle gap, *s*, when taking into account the 2D projection of AuNP dimers in cryo-EM images as discussed in the Supporting Information. The Gaussian distributions of *s* for the three DNA linker geometries are respectively centered on 7, 13, and 17.5 nm with standard deviations of 1, 2, and 3 nm. These values of *s* are estimated with error bars of the order of 1 and 0.5 nm for the

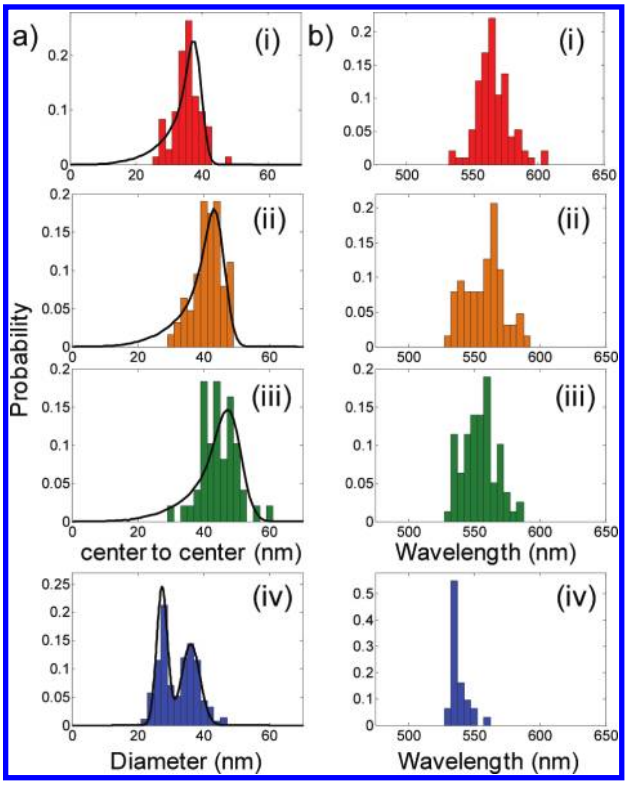

Figure 3. (a) Center to center distance (i−iii) and diameter (iv) distributions of the 27−36 nm AuNP dimer samples estimated from cryo-EM images. (b) Resonance wavelength distributions of single 36 nm AuNPs and symmetric dimers estimated from darkfield spectra of single scattering objects: (i) 50 bp DNA linker perpendicular to the dimer axis (red bars); (ii) 30 bp DNA linker parallel to the dimer axis (orange bars); (iii) 50 bp DNA linker parallel to the dimer axis (green bars); (iv) single particles. The black lines in panels a(i−iii) correspond to projected Gaussian distributions of the particle spacing, *s*, for the different samples (see text) and in panel a(iv) to Gaussian distributions of the particle diameters of 27 and 36 nm AuNPs. The bars in (a) and (b) are 2 and 5 nm wide, respectively.

distribution centers and standard deviations, respectively (see Supporting Information). They agree well with the interparticle distances expected from the shape of the organic scaffolds. Indeed, the lengths of 30 and 50 bp DNA double strands are 10 and 16.5 nm, respectively, while the width of a DNA double helix is about 2 nm. Furthermore, the length of the organic spacer linking the three thiol modifications to the end of the DNA strand and the length of the PEG shell are of the order of 2 nm.[32] The estimated gap values obtained from the fits in Figure 3a are thus close to the maximum expected interparticle gaps according to the scaffold geometries (6, 14, and 20.5 nm, respectively). This indicates that the net negative charges on the surface of the gold nanoparticles and of the DNA helix tend to stretch the overall nanostructure, especially for the samples reported in panels a (i) and a(ii) in Figure 3. For the sample in Figure 3a(i), it is possible that the DNA strand cannot hybridize over its whole length. It is important to note that the buffer solutions used for the cryo-EM and optical measurements contain reduced amounts of charge screening cations compared to previous reports[9,12,14] (around 1 mM NaCl) in order to maximize the rigidity of the DNA spacers. At these salt concentrations, the melting temperatures of the 30 bp and 50 bp sequences used in our experiments

dx.doi.org/10.1021/nl2032052 |*Nano Lett.* 2011, 11, 5060–5065

drop to 44 and 55 °C, respectively (as estimated using the Vector NTI software from Invitrogen), but allow the AuNP dimers to be stored at 8 °C and to be stable during the optical measurements at room temperature. The influence of NaCl concentration on the interparticle distance in DNA templated AuNP groupings has been discussed in the literature.[9,39] The particle spacing modification can be estimated in extended AuNP groupings using small-angle X-ray scattering.[39] For NaCl concentrations larger than 300 mM, the measured distances are shorter than what is expected for a fully extended DNA linker. However, at lower ionic strengths (50 mM NaCl), the groupings are stretched by electrostatic interactions with spacings consistent with the length of the DNA scaffold.[39] In the case of particle dimers, a plasmon resonance red shift can be observed when increasing the amount of charge screening cations in the buffer solution, evidencing reduced interparticle spacings.[9] These results are consistent with our observation of stretched dimers at low ionic strengths in the cryo-EM data of Figure 1. The widths of the distributions of interparticle distances observed in Figure 3a are thus due to varying particle diameters and to standard deviations of s that are of the order of 1, 2, and 3 nm for the three studied linker geometries.

To analyze the resonance wavelengths given in Figure 3b, we compare them to calculations performed with generalized Mie theory (GMT) to understand the origin of the large observed distribution width. This calculation method provides an analytical solution of Maxwell's equations for groupings of spheres in a homogeneous dielectric environment.[40−42] The analytical solution is solved numerically for a limited number of multipoles when the convergence is obtained. In the present case, the dielectric constant of gold is tabulated from published data[43] and the calculations are performed with up to 30 multipoles to obtain the resonance wavelength of the longitudinally coupled plasmon mode of AuNP dimers. Our optical experiments are performed in buffer solutions, but the gold particles are surrounded by organic material (PEG ligand shell, DNA linker, and protein functionalization of the glass substrates). The dielectric environment is therefore inhomogeneous with a value ranging between 1.33 (water) and 1.5 (typical organic medium). Figure 4a presents GMT calculations of the longitudinal resonance wavelength of 36 nm AuNP dimers versus the interparticle gap s for different dielectric environments. In Figure 4a, we also plot the experimental data of Figure 3b for the three dimer geometries. The spacing value and the horizontal error bar of each sample are taken from the center and standard deviation of the Gaussian fits of Figure 3a. The resonance wavelengths of the dimers and the error bars are estimated by fitting the distributions of Figure 3b with Gaussian distributions. Figure 4a shows that the evolution of the resonance wavelength for the different DNA linkers follows the theoretically expected behavior for an intermediate dielectric index between 1.33 and 1.5 (the red line at $n = 1.4$ is not the best fit scenario but provides a good agreement with experimental data).

One of the main advantages of GMT calculations is the high computation speed that allows the study of numerous parameter variations. Figure 4b presents estimated theoretical resonance wavelength distributions for the different DNA linkers and for single AuNPs using the Gaussian particle diameter and interparticle gap distributions estimated in cryo-EM. In this case, the surrounding dielectric index is chosen at $n = 1.4$. The centers of the theoretical distributions agree well with measured data, but the widths are much narrower than those experimentally observed.

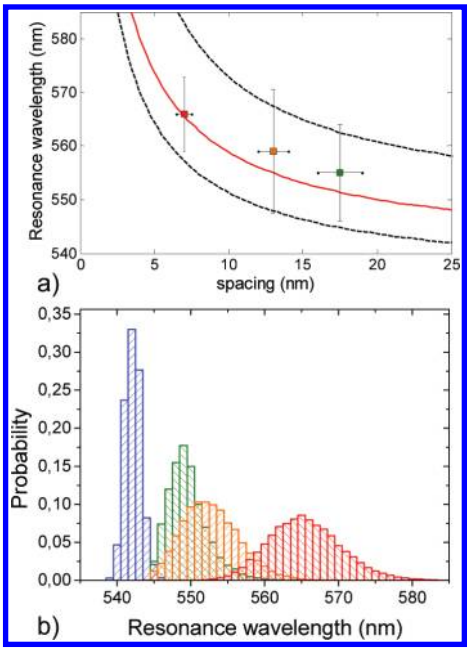

Figure 4. (a) Theoretical evolution of the longitudinal plasmon resonance wavelength of spherical 36 nm AuNP dimers versus spacing at different refractive indices compared to experimental data (see text). The bottom and top dotted lines correspond to refractive indices of 1.33 and 1.5, respectively. The solid red line corresponds to $n = 1.4$. (b) Theoretical resonance wavelength distributions estimated using GMT for spherical dimers using diameter and spacing distributions estimated in Figure 3a for the three dimer samples and single 36 nm particles for $n = 1.4$ (bar width is 1 nm): single AuNPs (blue stripes), 50 bp DNA linker parallel to the dimer axis (green stripes), 30 bp DNA linker parallel to the dimer axis (orange stripes), 50 bp DNA linker perpendicular to the dimer axis (red stripes).

The theoretical standard deviations are 2.5 times smaller for the single particles and the dimers of panels a(i) and b(i) of Figure 3, and nearly 4 times smaller for the dimers of panels a/b(ii) and a/b(iii) of Figure 3. The influence of the particle diameter distribution appears in Figure 4b for single particles but it is not sufficient to explain the measured wavelength distribution. Therefore, other factors such as local variations of the dielectric index and, more probably, the nonsphericity of the AuNPs must be taken into account as discussed previously in the literature.[11] This analysis thus indicates that the flexibility of the DNA linker, linked to the interparticle gap distributions, is only one of many contributing factors to the width of measured resonance wavelength distributions and is negligible for the dimers with larger spacings of panels a/b(ii) and a/b(iii) of Figure 3. Reducing the AuNP size and shape dispersion would be necessary to accurately estimate the influence of the DNA linker rigidity on the optical properties of the hybridized dimers.

This report demonstrates that it is possible to purify gold nanoparticles as large as 36 nm in diameter preferentially conjugated to a single DNA single strand as short as 10 nm. This allows us to synthesize high-purity suspensions of AuNP dimers with different DNA scaffolds. The distributions of interparticle gaps are estimated from cryo-EM images and by taking into account the AuNP diameter distributions and the orientation of the dimer versus the electron beam. In practice, the measured gaps are in good agreement with the size of the DNA linker and the length of the terminal thiol modifications. This analysis

dx.doi.org/10.1021/nl2032052 |*Nano Lett.* 2011, 11, 5060–5065

demonstrates that negatively charged particle dimers are observed in stretched geometries when analyzed in buffer solutions with low ionic strengths. Since the produced groupings are built with large particles and small gaps, the electromagnetic coupling of plasmonic modes in single dimers can be studied using confocal darkfield microscopy. The reduced particle spacings observed in cryo-EM are correlated to a red shift of the dimer resonance wavelength. The measured resonance frequency distributions are analyzed using generalized Mie theory calculations and demonstrate the limited effect of the DNA scaffold flexibility. Producing gold nanoparticle dimers with substantial scattering cross sections and a well-defined biochemical linker opens new perspectives on the design of higher efficiency sensors but also on the study of Raman scattering and fluorescence enhancements of single chromophores introduced specifically in the DNA sequence.

■ ASSOCIATED CONTENT

Supporting Information. DNA sequences, experimental procedures, and complementary characterization of particle dimers. This material is available free of charge via the Internet at http://pubs.acs.org/.

■ AUTHOR INFORMATION

Corresponding Author
*E-mail: sebastien.bidault@espci.fr.

■ ACKNOWLEDGMENT

The authors thank X. Z. Xu for dry TEM measurements, E. Bossy and E. Castanié for help with cryo-EM image analysis, G. Tessier and E. Fort for providing the imaging spectrometer, and K. Perronet for input on microchamber fabrication. Work at Institut Langevin was supported by a CNRS Grant "Interface Physique Chimie Biologie: Soutien à la prise de risque" and Agence Nationale de la Recherche via project ANR 11 BS10 002 02. Work at AMOLF is part of the research program of FOM which is financially supported by NWO and was also supported by NanoNed, a nanotechnology program of the Dutch ministry of Economic Affairs.

■ REFERENCES

(1) O'Neal, D. P.; Hirsch, L. R.; Halas, N. J.; Payne, J. D.; West, J. L. *Cancer Lett.* **2004**, *209*, 171–176.
(2) Huang, X. H.; El-Sayed, I. H.; Qian, W.; El-Sayed, M. A. *J. Am. Chem. Soc.* **2006**, *128*, 2115–2120.
(3) Schultz, S.; Smith, D. R.; Mock, J. J.; Schultz, D. A. *Proc. Natl. Acad. Sci. U.S.A.* **2000**, *97*, 996–1001.
(4) Warnasooriya, N.; Joud, F.; Bun, P.; Tessier, G.; Coppey-Moisan, M.; Desbiolles, P.; Atlan, M.; Abboud, M.; Gross, M. *Opt. Express* **2010**, *18*, 3264–3273.
(5) Alivisatos, A. P.; Johnsson, K. P.; Peng, X. G.; Wilson, T. E.; Loweth, C. J.; Bruchez, M. P.; Schultz, P. G. *Nature* **1996**, *382*, 609–611.
(6) Mirkin, C. A.; Letsinger, R. L.; Mucic, R. C.; Storhoff, J. J. A *Nature* **1996**, *382*, 607–609.
(7) Elghanian, R.; Storhoff, J. J.; Mucic, R. C.; Letsinger, R. L.; Mirkin, C. A. *Science* **1997**, *277*, 1078–1081.
(8) Liu, J. W.; Lu, Y. *Angew. Chem., Int. Ed.* **2006**, *45*, 90–94.
(9) Chen, J. I. L.; Chen, Y.; Ginger, D. S. *J. Am. Chem. Soc.* **2010**, *132*, 9600–9601.
(10) Sonnichsen, C.; Reinhard, B. M.; Liphardt, J.; Alivisatos, A. P. *Nat. Biotechnol.* **2005**, *23*, 741–745.
(11) Reinhard, B. M.; Siu, M.; Agarwal, H.; Alivisatos, A. P.; Liphardt, J. *Nano Lett.* **2005**, *5*, 2246–2252.
(12) Reinhard, B. M.; Sheikholeslami, S.; Mastroianni, A.; Alivisatos, A. P.; Liphardt, J. *Proc. Natl. Acad. Sci. U.S.A.* **2007**, *104*, 2667–2672.
(13) Skewis, L. R.; Reinhard, B. M. *Nano Lett.* **2008**, *8*, 214–220.
(14) Wang, H. Y.; Reinhard, B. M. *J. Phys. Chem. C* **2009**, *113*, 11215–11222.
(15) Graham, D.; Thompson, D. G.; Smith, W. E.; Faulds, K. *Nat. Nanotechnol.* **2008**, *3*, 548–551.
(16) Qian, X. M.; Zhou, S. M.; Nie, X *J. Am. Chem. Soc.* **2008**, *130*, 14934–14935.
(17) Lim, D. K.; Jeon, K. S.; Kim, H. M.; Nam, J. M.; Suh, Y. D. *Nat. Mater.* **2010**, *9*, 60–67.
(18) Zhang, J.; Fu, Y.; Chowdhury, M. H.; Lakowicz, J. R. *Nano Lett.* **2007**, *7*, 2101–2107.
(19) Zanchet, D.; Micheel, C. M.; Parak, W. J.; Gerion, D.; Alivisatos, A. P. *Nano Lett.* **2001**, *1*, 32–35.
(20) Claridge, S. A.; Liang, H. Y. W.; Basu, S. R.; Frechet, J. M. J.; Alivisatos, A. P. *Nano Lett.* **2008**, *8*, 1202–1206.
(21) Zanchet, D.; Micheel, C. M.; Parak, W. J.; Gerion, D.; Williams, S. C.; Alivisatos, A. P. *J. Phys. Chem. B* **2002**, *106*, 11758–11763.
(22) Claridge, S. A.; Goh, S. L.; Frechet, J. M. J.; Williams, S. C.; Micheel, C. M.; Alivisatos, A. P. *Chem. Mater.* **2005**, *17*, 1628–1635.
(23) Deng, Z. X.; Tian, Y.; Lee, S. H.; Ribbe, A. E.; Mao, C. D. *Angew. Chem., Int. Ed.* **2005**, *44*, 3582–3585.
(24) Sharma, J.; Chhabra, R.; Andersen, C. S.; Gothelf, K. V.; Yan, H.; Liu, Y. *J. Am. Chem. Soc.* **2008**, *130*, 7820–7821.
(25) Mastroianni, A. J.; Claridge, S. A.; Alivisatos, A. P. *J. Am. Chem. Soc.* **2009**, *131*, 8455–8459.
(26) Suzuki, K.; Hosokawa, K.; Maeda, M. *J. Am. Chem. Soc.* **2009**, *131*, 7518–7519.
(27) Bidault, S.; de Abajo, F. J. G.; Polman, A. *J. Am. Chem. Soc.* **2008**, *130*, 2750–2751.
(28) Aldaye, F. A.; Sleiman, H. F. *J. Am. Chem. Soc.* **2007**, *129*, 4130–4131.
(29) Rechberger, W.; Hohenau, A.; Leitner, A.; Krenn, J. R.; Lamprecht, B.; Aussenegg, F. R. *Opt. Commun.* **2003**, *220*, 137–141.
(30) Su, K. H.; Wei, Q. H.; Zhang, X.; Mock, J. J.; Smith, D. R.; Schultz, S. *Nano Lett.* **2003**, *3*, 1087–1090.
(31) Jain, P. K.; Huang, W. Y.; El-Sayed, M. A. *Nano Lett.* **2007**, *7*, 2080–2088.
(32) Li, Z.; Jin, R. C.; Mirkin, C. A.; Letsinger, R. L. *Nucleic Acids Res.* **2002**, *30*, 1558–1562.
(33) Li, H. X.; Rothberg, L. *Proc. Natl. Acad. Sci. U.S.A.* **2004**, *101*, 14036–14039.
(34) Li, H. X.; Rothberg, L. J. *J. Am. Chem. Soc.* **2004**, *126*, 10958–10961.
(35) Dubochet, J.; Lepault, J.; Freeman, R.; Berriman, J. A.; Homo, J. C. *J. Microsc.* **1982**, *128*, 219–237.
(36) Dubochet, J.; Adrian, M.; Chang, J. J.; Homo, J. C.; Lepault, J.; Mcdowall, A. W.; Schultz, P. *Q. Rev. Biophys.* **1988**, *21*, 129–228.
(37) Yang, L. L.; Wang, H. Y.; Yan, B.; Reinhard, B. M. *J. Phys. Chem. C* **2010**, *114*, 4901–4908.
(38) Sheikholeslami, S.; Jun, Y. W.; Jain, P. K.; Alivisatos, A. P. *Nano Lett.* **2010**, *10*, 2655–2660.
(39) Park, S. J.; Lazarides, A. A.; Storhoff, J. J.; Pesce, L.; Mirkin, C. A. *J. Phys. Chem. B* **2004**, *108*, 12375–12380.
(40) Stout, B.; Devilez, A.; Rolly, B.; Bonod, N. *J. Opt. Soc. Am. B* **2011**, *28*, 1213–1223.
(41) Lax, M. *Rev. Mod. Phys.* **1951**, *23*, 287–310.
(42) Wiscombe, W. J. *Appl. Opt.* **1980**, *19*, 1505–1509.
(43) Johnson, P. B.; Christy, R. W. *Phys. Rev. B* **1972**, *6*, 4370–4379.